Magnetospheric Accretion in Classical T Tauri Stars

J. Bouvier, S. H. P. Alencar
Laboratoire d'Astrophysique Grenoble

T. J. Harries
University of Exeter

C. M. Johns-Krull
Rice University

M. M. Romanova
Cornell University

The inner 0.1 AU around accreting T Tauri stars hold clues to many physical processes that characterize the early evolution of solar-type stars. The accretion-ejection connection takes place at least in part in this compact magnetized region around the central star, with the inner disk edge interacting with the star's magnetosphere thus leading simultaneously to magnetically channeled accretion flows and to high velocity winds and outflows. The magnetic star-disk interaction is thought to have strong implications for the angular momentum evolution of the central system, the inner structure of the disk, and possibly for halting the migration of young planets close to the stellar surface. We review here the current status of magnetic field measurements in T Tauri stars, the recent modeling efforts of the magnetospheric accretion process, including both radiative transfer and multi-D numerical simulations, and summarize current evidence supporting the concept of magnetically-channeled accretion in young stars. We also discuss the limits of the models and highlight observational results which suggest that the star-disk interaction is a highly dynamical and time variable process in young stars.

1. THE MAGNETIC ACCRETION PARADIGM

T Tauri stars are low-mass stars with an age of a few million years, still contracting down their Hayashi tracks towards the main sequence. Many of them, the so-called classical T Tauri stars (CTTSs), show signs of accretion from a circumstellar disk (see, e.g., *Ménard and Bertout*, 1999 for a review). Understanding the accretion process in T Tauri stars is one of the major challenges in the study of pre-main sequence evolution. Indeed, accretion has a significant and long lasting impact on the evolution of low mass stars by providing both mass and angular momentum. The evolution and ultimate fate of circumstellar accretion disks have also become increasingly important issues since the discovery of extrasolar planets and planetary systems with unexpected properties. Deriving the properties of young stellar systems, of their associated disks and outflows is therefore an important step towards the establishment of plausible scenarios for star and planet formation.

The general paradigm of magnetically controlled accretion onto a compact object is used to explain many of the most fascinating objects in the Universe. This model is a seminal feature of low mass star formation, but it is also encountered in theories explaining accretion onto white dwarf stars (the AM Her stars, e.g., *Warner*, 2004), accretion

onto pulsars (the pulsating X-ray sources , e.g., *Ghosh and Lamb*, 1979a), and accretion onto black holes at the center of AGNs and microquasars (*Koide et al.*, 1999). Strong surface magnetic fields have long been suspected to exist in TTSs based on their powerful X-ray and centrimetric radio emissions (*Montmerle et al.*, 1983; *André*, 1987). Surface fields of order of 1-3 kG have recently been derived from Zeeman broadening measurements of CTTS photospheric lines (*Johns Krull et al.*, 1999a, 2001; *Guenther et al.*, 1999) and from the detection of electron cyclotron maser emission (*Smith et al.*, 2003). These strong stellar magnetic fields are believed to significantly alter the accretion flow in the circumstellar disk close to the central star.

Based on models originally developed for magnetized compact objects in X-ray pulsars (*Ghosh and Lamb*, 1979a) and *assuming* that T Tauri magnetospheres are predominantly dipolar on the large scale, *Camenzind* (1990) and *Königl* (1991) showed that the inner accretion disk is expected to be truncated by the magnetosphere at a distance of a few stellar radii above the stellar surface for typical mass accretion rates of 10^{-9} to 10^{-7} $M_\odot$ yr^{-1} in the disk (*Basri and Bertout*, 1989; *Hartigan et al.*, 1995; *Gullbring et al.*, 1998). Disk material is then channeled from the disk inner edge onto the star along the magnetic field lines, thus giving rise to magnetospheric accretion columns. As the

free falling material in the funnel flow eventually hits the stellar surface, accretion shocks develop near the magnetic poles. The basic concept of magnetospheric accretion in T Tauri stars is illustrated in Figure 1.

The successes and limits of current magnetospheric accretion models in accounting for the observed properties of classical T Tauri systems are reviewed in the next sections. Sect. 2 summarizes the current status of magnetic field measurements in young stars, Sect. 3 provides an account of current radiative transfer models developed to reproduce the observed line profiles thought to form at least in part in accretion funnel flows, Sect. 4 reviews current observational evidence for a highly dynamical magnetospheric accretion process in CTTSs, and Sect. 5 describes the most recent 2D and 3D numerical simulations of time dependent star-disk magnetic interaction.
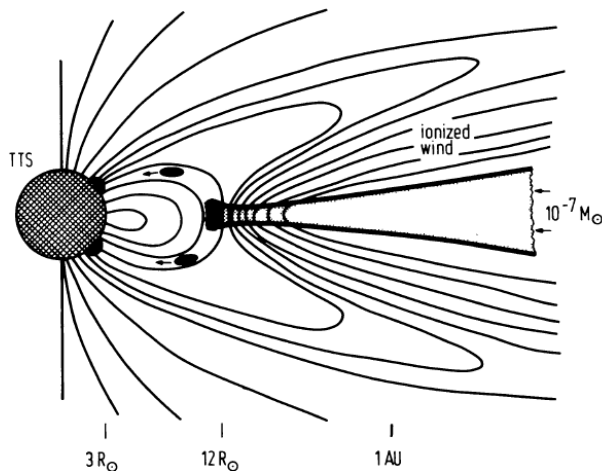

Fig. 1.— A sketch of the basic concept of magnetospheric accretion in T Tauri stars (from *Camenzind*, 1990).

2. MAGNETIC FIELD MEASUREMENTS

2.1. Theoretical Expectations for T Tauri Magnetic Fields

While the interaction of a stellar magnetic field with an accretion disk is potentially very complicated (e.g., *Ghosh and Lamb*, 1979a,b), we present here some results from the leading treatments applied to young stars.

The theoretical idea behind magnetospheric accretion is that the ram pressure of the accreting material ($P_{ram} = 0.5\rho v^2$) will at some point be offset by the magnetic pressure ($P_B = B^2/8\pi$) for a sufficiently strong stellar field. Where these two pressures are equal, if the accreting material is sufficiently ionized, its motion will start to be controlled by the stellar field. This point is usually referred to as the truncation radius (R_T). If we consider the case of spherical accretion, the magnetic field becomes

$$B^2 = \frac{\dot{M}v}{r^2}. \tag{2.1}$$

If we then assume a dipolar stellar magnetic field where $B = B_*(R_*/r)^3$ and set the velocity of the accreting material equal to the free-fall speed, the radius at which the magnetic field pressure balances the ram pressure of the accreting material is

$$\frac{R_T}{R_*} = \frac{B_*^{4/7} R_*^{5/7}}{\dot{M}^{2/7}(2GM_*)^{1/7}} = 7.1 B_3^{4/7} \dot{M}_{-8}^{-2/7} M_{0.5}^{-1/7} R_2^{5/7}, \tag{2.2}$$

where B_3 is the stellar field strength in kG, $\dot{M}_{-8}$ is the mass accretion rate in units of 10^{-8} M$_\odot$ yr^{-1}, $M_{0.5}$ is the stellar mass in units of 0.5 M$_\odot$, and R_2 is the stellar radius in units of 2 R$_\odot$. Then, for $B_* = 1$ kG and typical CTTS properties ($M_* = 0.5$ M$_\odot$, $R_* = 2$ R$_\odot$, and $\dot{M} = 10^{-8}$ M$_\odot$ yr^{-1}), the truncation radius is about 7 stellar radii.

In the case of disk accretion, the coefficient above is changed, but the scaling with the stellar and accretion parameters remains the same. In accretion disks around young stars, the radial motion due to accretion is relatively low while the Keplerian velocity due to the orbital motion is only a factor of $2^{1/2}$ lower than the free-fall velocity. The low radial velocity of the disk means that the disk densities are much higher than in the spherical case, so that the disk ram pressure is higher than the ram pressure due to spherical free-fall accretion. As a result, the truncation radius will move closer to the star. In this regard, equation 2.2 gives an upper limit for the truncation radius. As we will discuss below, this may be problematic when we consider the current observations of stellar magnetic fields. In the case of disk accretion, another important point in the disk is the corotation radius, R_{CO}, where the Keplerian angular velocity is equal to the stellar angular velocity. Stellar field lines which couple to the disk outside of R_{CO} will act to slow the rotation of the star down, while field lines which couple to the disk inside R_{CO} will act to spin the star up. Thus, the value of R_T relative to R_{CO} is an important quantity in determining whether the star speeds up or slows down its rotation. For accretion onto the star to proceed, we have the relation $R_T < R_{CO}$. This follows from the idea that at the truncation radius and interior to that, the disk material will be locked to the stellar field lines and will move at the same angular velocity as the star. Outside R_{CO} the stellar angular velocity is greater than the Keplerian velocity, so that any material there which becomes locked to the stellar field will experience a centrifugal force that tries to fling the material away from the star. Only inside R_{CO} will the net force allow the material to accrete onto the star.

Traditional magnetospheric accretion theories as applied to stars (young stellar objects, white dwarfs, and pulsars) suggest that the rotation rate of the central star will be set by the Keplerian rotation rate in the disk near the point where the disk is truncated by the stellar magnetic field when the system is in equilibrium. Hence these theories are often referred to as disk locking theories. For CTTSs, we have a unique opportunity to test these theories since all the variables of the problem (stellar mass, radius, rotation rate, magnetic field, and disk accretion rate) are mea-

sureable in principle (see *Johns–Krull and Gafford*, 2002). Under the assumption that an equilibrium situation exists, *Königl* (1991), *Cameron and Campbell* (1993), and *Shu et al.* (1994) have all analytically examined the interaction between a dipolar stellar magnetic field (aligned with the stellar rotation axis) and the surrounding accretion disk. As detailed in *Johns–Krull et al.* (1999b), one can solve for the surface magnetic field strength on a CTTS implied by each of these theories given the stellar mass, radius, rotation period, and accretion rate. For the work of *Königl* (1991), the resulting equation is:

$$B_* = 3.43 \left(\frac{\epsilon}{0.35}\right)^{7/6} \left(\frac{\beta}{0.5}\right)^{-7/4} \left(\frac{M_*}{M_\odot}\right)^{5/6} \times$$

$$\times \left(\frac{\dot{M}}{10^{-7}\ M_\odot\ \mathrm{yr}^{-1}}\right)^{1/2} \left(\frac{R_*}{R_\odot}\right)^{-3} \left(\frac{P_*}{1\ \mathrm{dy}}\right)^{7/6}\ \mathrm{kG}, \quad (2.3)$$

In the work of *Cameron and Campbell* (1993) the equation for the stellar field is:

$$B_* = 1.10\gamma^{-1/3} \left(\frac{M_*}{M_\odot}\right)^{2/3} \left(\frac{\dot{M}}{10^{-7}\ M_\odot\ \mathrm{yr}^{-1}}\right)^{23/40} \times$$

$$\times \left(\frac{R_*}{R_\odot}\right)^{-3} \left(\frac{P_*}{1\ \mathrm{dy}}\right)^{29/24}\ \mathrm{kG}, \quad (2.4)$$

Finally, from *Shu et al.* (1994), the resulting equation is:

$$B_* = 3.38 \left(\frac{\alpha_x}{0.923}\right)^{-7/4} \left(\frac{M_*}{M_\odot}\right)^{5/6} \left(\frac{\dot{M}}{10^{-7}\ M_\odot\ \mathrm{yr}^{-1}}\right)^{1/2} \times$$

$$\times \left(\frac{R_*}{R_\odot}\right)^{-3} \left(\frac{P_*}{1\ \mathrm{dy}}\right)^{7/6}\ \mathrm{kG}, \quad (2.5)$$

All these equations contain uncertain scaling parameters ($\epsilon, \beta, \gamma, \alpha_x$) which characterize the efficiency with which the stellar field couples to the disk or the level of vertical shear in the disk. Each study presents a best estimate for these parameters allowing the stellar field to be estimated (Table 1). Observations of magnetic fields on CTTSs can then serve as a test of these models.

To predict magnetic field strengths for specific CTTSs, we need observational estimates for certain system parameters. We adopt rotation periods from *Bouvier et al.* (1993, 1995) and stellar masses, radii, and mass accretion rates from *Gullbring et al.* (1998). Predictions for each analytic study are presented in Table 1. Note, these field strengths are the equatorial values. The field at the pole will be twice these values and the average over the star will depend on the exact inclination of the dipole to the observer, but for $i = 45°$ the average field strength on the star is ~ 1.4 times the values given in the Table. Because of differences in underlying assumptions, these predictions are not identical, but they do have the same general dependence on system characteristics. Consequently, field strengths predicted by the 3 theories, while different in scale, nonetheless have the same pattern from star to star. Relatively weak fields are predicted for some stars (DN Tau, IP Tau), but detectably strong fields are expected on stars such as BP Tau.

2.2. Measurement Techniques

Virtually all measurements of stellar magnetic fields make use of the Zeeman effect. Typically, one of two general aspects of the Zeeman effect is utilized: (1) Zeeman broadening of magnetically sensitive lines observed in intensity spectra, or (2) circular polarization of magnetically sensitive lines. Due to the nature of the Zeeman effect, the splitting due to a magnetic field is proportional to λ^2 of the transition. Compared with the λ^1 dependence of Doppler line broadening mechanisms, this means that observations in the infrared (IR) are generally more sensitive to the presence of magnetic fields than optical observations.

The simplest model of the spectrum from a magnetic star assumes that the observed line profile can be expressed as $F(\lambda) = F_B(\lambda) * f + F_Q(\lambda) * (1 - f)$; where F_B is the spectrum formed in magnetic regions, F_Q is the spectrum formed in non-magnetic (quiet) regions, and f is the flux weighted surface filling factor of magnetic regions. The magnetic spectrum, F_B, differs from the spectrum in the quiet region not only due to Zeeman broadening of the line, but also because magnetic fields affect atmospheric structure, causing changes in both line strength and continuum intensity at the surface. Most studies *assume* that the magnetic atmosphere is in fact the same as the quiet atmosphere because there is no theory to predict the structure of the magnetic atmosphere. If the stellar magnetic field is very strong, the splitting of the σ components is a substantial fraction of the line width, and it is easy to see the σ components sticking out on either side of a magnetically sensitive line. In this case, it is relatively straightforward to measure the magnetic field strength, B. Differences in the atmospheres of the magnetic and quiet regions primarily affect the value of f. If the splitting is a small fraction of the intrinsic line width, then the resulting observed profile is only subtly different from the profile produced by a star with no magnetic field and more complicated modelling is required to be sure all possible non-magnetic sources (e.g., rotation and pressure broadening) have been properly constrained.

In cases where the Zeeman broadening is too subtle to detect directly, it is still possible to diagnose the presence of magnetic fields through their effect on the equivalent width of magnetically sensitive lines. For strong lines, the Zeeman effect moves the σ components out of the partially saturated core into the line wings where they can effectively add opacity to the line and increase the equivalent width. The exact amount of equivalent width increase is a complicated function of the line strength and Zeeman splitting pattern (*Basri et al.*, 1992). This method is primarily sensitive to the product of B multiplied by the filling factor f (*Basri et al.*, 1992, *Guenther et al.*, 1999). Since this method relies on relatively small changes in the line equivalent width, it is very important to be sure other atmospheric parameters which affect equivalent width (particularly temperature) are accurately measured.

Measuring circular polarization in magnetically sensitive lines is perhaps the most direct means of detecting magnetic

TABLE 1

PREDICTED MAGNETIC FIELD STRENGTHS

Star	M_* $(M_\odot)$	R_* $(R_\odot)$	$\dot{M} \times 10^8$ $(M_\odot \mathrm{yr}^{-1})$	P_{rot} (days)	B_*^a (G)	B_*^b (G)	B_*^c (G)	R_{CO} (R_*)	$\bar{B}_{obs}$ (kG)
AA Tau	0.53	1.74	0.33	8.20	810	240	960	8.0	2.57
BP Tau	0.49	1.99	2.88	7.60	1370	490	1620	6.4	2.17
CY Tau	0.42	1.63	0.75	7.90	1170	390	1380	7.7	
DE Tau	0.26	2.45	2.64	7.60	420	164	490	4.2	1.35
DF Tau	0.27	3.37	17.7	8.50	490	220	570	3.4	2.98
DK Tau	0.43	2.49	3.79	8.40	810	300	950	5.3	2.58
DN Tau	0.38	2.09	0.35	6.00	250	80	300	4.8	2.14
GG Tau A	0.44	2.31	1.75	10.30	890	320	1050	6.6	1.57
GI Tau	0.67	1.74	0.96	7.20	1450	450	1700	7.9	2.69
GK Tau	0.46	2.15	0.64	4.65	270	90	320	4.2	2.13
GM Aur	0.52	1.78	0.96	12.00	1990	660	2340	10.0	
IP Tau	0.52	1.44	0.08	3.25	240	60	280	5.2	
TW Hya	0.70	1.00	0.20	2.20	900	240	1060	6.3	2.61
T Tau	2.11	3.31	4.40	2.80	390	110	460	3.2	2.39

NOTE.—Magnetic field values come from applying the theory of (*a*) *Könignl* (1991), (*b*) *Cameron and Campbell*, or (*c*) *Shu et al.* (1994). These are the equatorial field strengths assuming a dipole magnetic field.

fields on stellar surfaces, but is also subject to several limitations. When viewed along the axis of a magnetic field, the Zeeman σ components are circularly polarized, but with opposite helicity; and the π component is absent. The helicity of the σ components reverses as the polarity of the field reverses. Thus, on a star like the Sun that typically displays equal amounts of $+$ and $-$ polarity fields on its surface, the net polarization is very small. If one magnetic polarity does dominate the visible surface of the star, net circular polarization is present in Zeeman sensitive lines, resulting in a wavelength shift between the line observed through right- and left-circular polarizers. The magnitude of the shift represents the surface averaged line of sight component of the magnetic field (which on the Sun is typically less than 4 G even though individual magnetic elements on the solar surface range from ~ 1.5 kG in plages to ~ 3.0 kG in spots). Several polarimetric studies of cool stars have generally failed to detect circular polarization, placing limits on the disk-averaged magnetic field strength present of $10 - 100$ G (e.g., *Vogt*, 1980; *Brown and Landstreet*, 1981; *Borra et al.*, 1984). One notable exception is the detection of circular polarization in segments of the line profile observed on rapidly rotating dwarfs and RS CVn stars where Doppler broadening of the line "resolves" several independent strips on the stellar surface (e.g., *Donati et al.*, 1997; *Petit et al.*, 2004; *Jardine et al.*, 2002).

2.3. Mean Magnetic Field Strength

TTS typically have $v \sin i$ values of 10 km s^{-1}, which means that observations in the optical typically cannot detect the actual Zeeman broadening of magnetically sensitive lines because the rotational broadening is too strong. Nevertheless, optical observations can be used with the equivalent width technique to detect stellar fields. *Basri et al.* (1992) were the first to detect a magnetic field on the surface of a TTS, inferring a value of $Bf = 1.0$ kG on the NTTS Tap 35. For the NTTS Tap 10, *Basri et al.* (1992) find only an upper limit of $Bf < 0.7$ kG. *Guenther et al.* (1999) apply the same technique to spectra of 5 TTSs, claiming significant field detections on two stars; however, these authors analyze their data using models off by several hundred K from the expected effective temperature of their target stars, always a concern when relying on equivalent widths.

As we saw above, observations in the IR will help solve the difficulty in detecting direct Zeeman broadening. For this reason and given the temperature of most TTSs (K7 - M2), Zeeman broadening measurements for these stars are best done using several Ti I lines found in the K band. Robust Zeeman broadening measurements require Zeeman insensitive lines to constrain nonmagnetic broadening mechanisms. Numerous CO lines at 2.31 μm have negligible Landé-g factors, making them an ideal null reference.

It has now been shown that the Zeeman insensitive CO lines are well fitted by models with the same level of rotational broadening as that determined from optical line pro-

files (*Johns–Krull and Valenti*, 2001; *Johns–Krull et al.*, 2004; *Yang et al.*, 2005). In contrast, the 2.2 μm Ti I lines cannot be fitted by models without a magnetic field. Instead, the observed spectrum is best fit by a model with a superposition of synthetic spectra representing different regions on the star with different magnetic field strengths. Typically, the field strengths in these regions are assumed to have values of 0, 2, 4, and 6 kG and only the filling factor of each region is solved for. The resulting magnetic field distribution is unique because the Zeeman splitting produced by a 2 kG field is comparable to the nonmagnetic width of the Ti I spectral lines. In other words, the Zeeman resolution of the Ti I lines is about 2 kG (see *Johns–Krull et al.*, 1999b, 2004).

The intensity-weighted mean magnetic field strength, $\bar{B}$, over the entire surface of most TTSs analyzed to date is ~ 2.5 kG, with field strengths reaching at least 4 kG and probably even 6 kG in some regions. Thus, magnetic fields on TTSs are stronger than on the Sun, even though the surface gravity on these stars is lower by a factor of ten. On the Sun and other main-sequence stars, magnetic field strength seems to be set by an equipartition of gas and magnetic pressure. In contrast, the photospheres of TTSs are apparently dominated by magnetic pressure, rather than gas pressure (see also *Johns–Krull et al.*, 2004). Strong magnetic fields are ubiquitous on TTSs. By fitting IR spectra, magnetic field distributions for several TTSs have now been measured (*Johns–Krull et al.*, 1999b, 2001, 2004; *Yang et al.*, 2005). Many of these field strengths are reported in Table 1.

2.4. Magnetic Field Topology

Zeeman broadening measurements are sensitive to the distribution of magnetic field strengths, but they have limited sensitivity to magnetic geometry. In contrast, circular polarization measurements for individual spectral lines are sensitive to magnetic geometry, but they provide limited information about field strength. The two techniques complement each other well, as we demonstrate below.

Most existing magnetospheric accretion models assume that intrinsic TTS magnetic fields are dipolar, but this would be unprecedented for cool stars. The higher order components of a realistic multi-polar field will fall off more rapidly with distance than the dipole component, so at the inner edge of the disk a few stellar radii from the surface, it is likely the dipolar component of the stellar field will dominate. However, at the stellar surface the magnetic field is likely to be more complicated. In support of this picture is the fact that spectropolarimetric observations do not detect polarization in photospheric absorption lines: *Brown and Landstreet* (1981) failed to detect polarization in T Tau and two FU Ori objects; *Johnstone and Penston* (1986) observed 3 CTTSs and reported a marginal field detection for RU Lup, but they were not able to confirm the signal in a subsequent observation, perhaps because of rotational modulation (*Johnstone and Penston*, 1987); *Donati et al.* (1997)
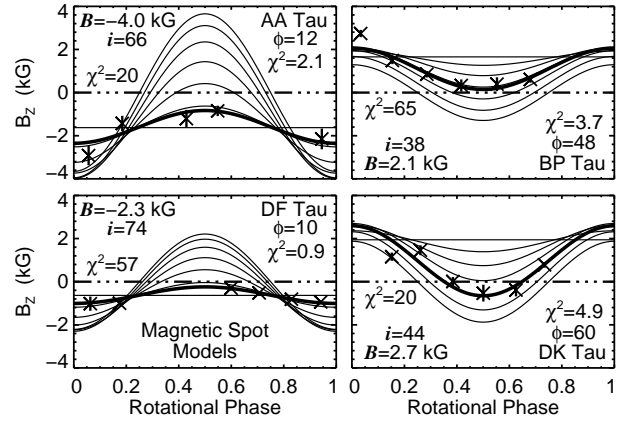

Fig. 2.— Variations in the circular polarization of the He I emission line as a function of rotation phase for 4 CTTSs. Polarization levels are translated into B_z values in the line formation region. Vertical bars centered on each measurement ($\times$) give the 1σ uncertainty in the field measurement. Solid lines show predicted rotational modulation in B_z for a single magnetic spot at latitudes (ϕ) ranging from $0°$ to $90°$ in $15°$ increments. The best fit latitude is shown in the thick solid curve.

find no evidence for a strong dipolar field component in the 3 TTSs they observed; *Johns–Krull et al.* (1999a) failed to detect polarization in the photospheric lines of BP Tau; and *Valenti and Johns–Krull* (2004) do not detect significant polarization in the photospheric lines of 4 CTTSs each observed over a rotation period. *Smirnov et al.* (2003) report a marginal detection of circular polarization in the lines of T Tau corresponding to a field of $\sim 150 \pm 50$ G; however, *Smirnov et al.* (2004) and *Daou et al.* (2005) failed to confirm this detection, placing an upper limit on the field of ≤ 120 G for T Tau.

However, *Johns–Krull et al.* (1999a) did discover circular polarization in CTTS emission line diagnostics that form predominantly in the accretion shock at the surface of the star. This circular polarization signal is strongest in the narrow component of the He I 5876 Å emission line, but it is also present in the Ca I infrared triplet lines. The peak value of B_z is 2.5 kG, which is comparable to our measured values of $\bar{B}$. Circular polarization in the He I 5876 Å emission line has now been observed in a number of CTTSs (*Valenti et al.*, 2004; *Symington et al.*, 2005b). Note, since this polarization is detected in a line associated with the accretion shock on CTTSs, it forms over an area covering typically $< 5\%$ of the stellar surface (*Valenti et al.*, 1993; *Calvet and Gullbring*, 1998). While the field in this 5% of the star appears to be highly organized (and as discussed below may trace the dipole component of the field at the surface), the lack of polarization detected in photospheric lines forming over the entire surface of the star strongly rule out a global dipole geometry for the entire field.

Figure 2 shows measurements of B_z on 6 consecutive nights. These measurements were obtained at McDon-

ald Observatory, using the Zeeman analyzer described by *Johns–Krull et al.* (1999a). The measured values of B_z vary smoothly on rotational timescales, suggesting that uniformly oriented magnetic field lines in accretion regions sweep out a cone in the sky, as the star rotates. Rotational modulation implies a lack of symmetry about the rotation axis in the accretion or the magnetic field or both. For example, the inner edge of the disk could have a concentration of gas that corotates with the star, preferentially illuminating one sector of a symmetric magnetosphere. Alternatively, a single large scale magnetic loop could draw material from just one sector of a symmetric disk.

Figure 2 shows one interpretation of the He I polarization data. Predicted values of B_z are shown for a simple model consisting of a single magnetic spot at latitude ϕ that rotates with the star. The magnetic field is assumed to be radial with a strength equal to our measured values of $\bar{B}$. Inclination of the rotation axis is constrained by measured $v \sin i$ and rotation period, except that inclination (i) is allowed to float when it exceeds $60°$ because $v \sin i$ measurements cannot distinguish between these possibilities. Predicted variations in B_z are plotted for spot latitudes ranging from $0°$ to $90°$ in $15°$ increments. The best fitting model is shown by the thick curve. The corresponding spot latitude and reduced χ^2 are given on the right side of each panel. The null hypothesis (that no polarization signal is present) produces very large values of χ^2 which are given on the left side of each panel. In all four cases, this simple magnetic spot model reproduces the observed B_z time series. The He I rotationally modulated polarization combined with the lack of detectable polarization in photospheric absorption lines as described above paints a picture in which the magnetic field on TTSs displays a complicated geometry at the surface which gives way to a more ordered, dipole-like geometry a few stellar radii from the surface where the field intersects the disk. The complicated surface topology results in no net polarization in photospheric absorption lines, but the dipole-like geometry of the field at the inner disk edge means that accreting material follows these field lines down to the surface so that emission lines formed in the accretion shock preferentially illuminate the dipole component of the field, producing substantial circular polarization in these emission lines.

2.5. Confronting Theory with Observations

At first glance, it might appear that magnetic field measurements on TTS are generally in good agreement with theoretical expectations. Indeed, the IR Zeeman broadening measurements indicate mean fields on several TTSs of ~ 2 kG, similar in value to those predicted in Table 1 (recall the field values in the Table are the equatorial values for a dipolar field, and that the mean field is about 1.5 times these equatorial values). However, in detail the field observations do not agree with the theory. This can be seen in Figure 3, where we plot the measured magnetic field strengths versus the predicted field strengths from *Shu et al.* (1994, see
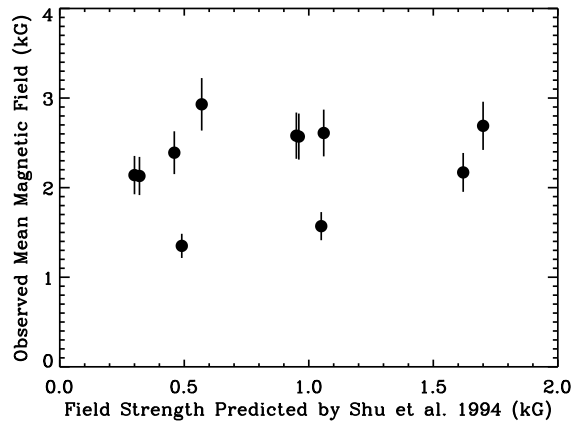

Fig. 3.— Observed mean magnetic field strength determined from IR Zeeman broadening measurements as a function of the predicted field strength from Table 1 for the theory of *Shu et al.* (1994). No statistically significant correlation is found between the observed and predicted field strengths.

Table 1). Clearly, the measured field strengths show no correlation with the predicted field strengths. The field topology measurements give some indication to why there may be a lack of correlation: the magnetic field on TTSs are not dipolar, and the dipole component to the field is likely to be a factor of ~ 10 or more lower than the values predicted in Table 1. As discussed in *Johns–Krull et al.* (1999b), the 3 studies which produce the field predictions in Table 1 involve uncertain constants which describe the efficiency with which stellar field lines couple to the accretion disk. If these factors are much different than estimated, it may be that the required dipole components to the field are substantially less than the values given in the Table. On the other hand, equation 2.2 was derived assuming perfect coupling of the field and the matter, so it serves as a firm upper limit to R_T as discussed in §2.1. Spectropolarimetry of TTSs indicates that the dipole component of the magnetic field is ≤ 0.1 kG (*Valenti and Johns–Krull*, 2004; *Smirnov et al.*, 2004; *Daou et al.*, 2005). Putting this value into equation 2.2, we find $R_T \leq 1.9 \, R_*$ for typical CTTS parameters. Such a low value for the truncation radius is incompatible with rotation periods of 7-10 days as found for many CTTS (Table 1 and, e.g., *Herbst et al.*, 2002).

Does this then mean that magnetospheric accretion does not work? Independent of the coupling efficiency between the stellar field and the disk, magnetospheric accretion models predict correlations between stellar and accretion parameters. As shown in §2.3, the fields on TTS are found to all be rather uniform in strength. Eliminating the stellar field then, *Johns–Krull and Gafford* (2002) looked for correlation among the stellar and accretion parameters, finding little evidence for the predicted correlations. This absence of

the expected correlations had been noted earlier by *Muzerolle et al.* (2001). On the other hand, *Johns–Krull and Gafford* (2002) showed how the models of *Ostriker and Shu* (1995) could be extended to take into account non-dipole field geometries. Once this is done, the current data do reveal the predicted correlations, suggesting magnetospheric accretion theory is basically correct as currently formulated. So then, how do we reconcile the current field measurements with this picture? While the dipole component of the field is small on TTSs, it is clear the stars posses strong fields over most, if not all, of their surface but with a complicated surface topology. Perhaps this can lead to a strong enough field so that $R_T \sim 6\ R_*$ as generally suggested by observations of CTTS phenomena. More complicated numerical modelling of the interaction of a complex geometry field with an accretion disk will be required to see if this is feasible.

3. SPECTRAL DIAGNOSTICS OF MAGNETOSPHERIC ACCRETION

Permitted emission line profiles from CTTSs, in particular the Balmer series, show a wide variety of morphologies including symmetric, double-peaked, P Cygni, and inverse P Cygni (IPC) type (*Edwards et al.*, 1994): common to all shapes is a characteristic line width indicative of bulk motion within the circumstellar material of hundreds of km s^{-1}. The lines themselves encode both geometrical and physical information on the accretion process and its rate, and the challenge is to use the profiles to test and refine the magnetospheric accretion model.

Interpretation of the profiles requires a translational step between the physical model and the observable spectra; this is the process of radiative-transfer (RT) modelling. The magnetospheric accretion paradigm presents a formidable problem in RT, since the geometry is two or three dimensional, the material is moving, and the radiation-field and the accreting gas are decoupled (i.e. the problem is non-LTE). However, the past decade has seen the development of increasingly sophisticated RT models that have been used to model line profiles (both equivalent width and shape) in order to determine accretion rates. In this section we describe the development of these models, and characterize their successes and failures.

Current models are based on idealized axisymmetric geometry, in which the circumstellar density structure is calculated assuming free-fall along dipolar field lines that emerge from a geometrically thin disc at a range of radii encompassing the corotation radius. It is assumed that the kinetic energy of the accreting material is completely thermalized, and that the accretion luminosity, combined with the area of the accretion footprints (rings) on the stellar surface, provide the temperature of the hot spots. The circumstellar density and velocity structure is then fully described by the mass accretion rate, and the outer and inner radii of

the magnetosphere in terms of the photospheric radius of the star (*Hartmann et al.*, 1994).

A significant, but poorly constrained, input parameter for the models is the temperature structure of the accretion flow. This is a potential pitfall, as the form of the temperature structure may have a significant impact on the line source functions, and therefore the line profiles themselves. Self-consistent radiative equilibrium models (*Martin*, 1996) indicate that adiabatic heating and cooling via bremsstrahlung dominate the thermal budget, whereas Hartmann and coworkers adopt a simple volumetric heating rate combined with a schematic radiative cooling rate which leads to a temperature structure that goes as the reciprocal of the density. Thus the temperature is low near the disc, and passes through a maximum (as the velocity increases and density decreases) before the stream cools again as it approaches the stellar surface (and the density increases once more).

With the density, temperature and velocity structure of the accreting material in place, the level populations of the particular atom under consideration must be calculated under the constraint of statistical equilibrium. This calculation is usually performed using the Sobolev approximation, in which it is assumed that the conditions in the gas do not vary significantly over a length scale given by

$$l_S = v_{therm}/(dv/dr) \tag{1}$$

where v_{therm} is the thermal velocity of the gas and dv/dr is the velocity gradient. Such an approximation is only strictly valid in the fastest parts of the accretion flow. Once the level populations have converged, the line opacities and emissivities are then computed, allowing the line profile of any particular transition to be calculated.

The first models computed using the method outlined above were presented by *Hartmann et al.* (1994), who adopted a two-level atom approximation. It was demonstrated that the magnetospheric accretion model could reproduce the main characteristics of the profiles, including IPC profiles and blue-shifted central emission peaks. The original Hartmann et al. model was further improved by *Muzerolle et al.* (2001). Instead of using a two-level approximation, they solved statistical equilibrium (still under Sobolev) for a 20-level hydrogen atom. Their line profiles were computed using a direct integration method, which, unlike the Sobolev approach, allows the inclusion of Stark broadening effects. It was found that the broadening was most significant for Hα, with the line reaching widths of ~ 500 km s^{-1}, a width that significantly exceeds the doppler broadening due to infall alone, and in much better agreement with observation. The Hβ model profiles were found to be in broad agreement with the observations, in terms of the velocity of the emission peak (*Alencar and Basri*, 2000), and in the asymmetry of the profiles (*Edwards et al.*, 1994). Figure 4 shows model Hα profiles as a function of mass accretion rate and accretion flow temperature; one can see that for typical CTTS accretion rates the line profiles are broadly symmetric although slightly blueshifted
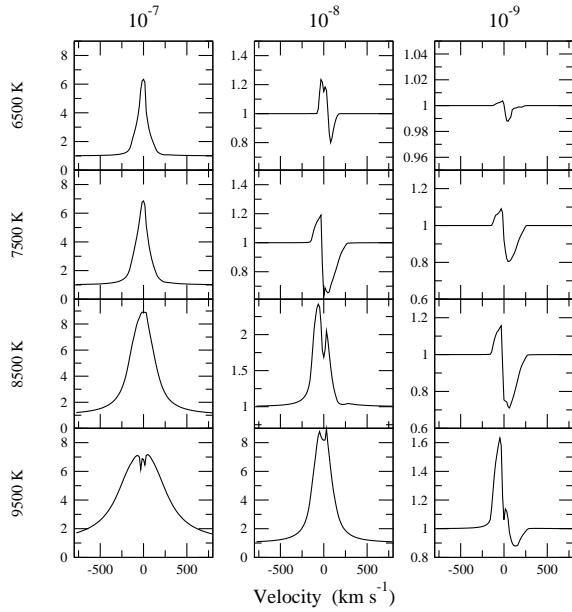
Fig. 4.— Hα model profiles for a wide range of mass accretion rate and accretion flow maximum temperature (from *Kurosawa et al.*, 2006). The profiles are based on canonical CTTS parameters ($R = 2\,R_\odot$, $M = 0.5\,M_\odot$, $T = 4000$ K) viewed at an inclination of $55°$. The maximum temperature of the accretion flow is indicated along the left of the figure, while the accretion rate (in $M_\odot\,\mathrm{yr}^{-1}$) is shown along the top.

Fig. 5.— Sample Hα model profiles (*Kurosawa et al.*, 2006) which characterize the morphological classification (Types I-IV B/R) by *Reipurth et al.* (1996). The combination of magnetospheric accretion, the accretion disc, and the collimated disk wind can reproduce the wide range of Hα profiles seen in observations. The horizontal axes are velocities in $\mathrm{km\,s}^{-1}$ and the vertical axes are continuum normalized intensities.

– the reduced optical depth for the lower accretion rate models yields the IPC morphology.

Axisymmetric models are obviously incapable of reproducing the wide range of variability that is observed in the emission lines of CTTSs (Sect. 4). Although the addition of further free parameters to models naturally renders them more arbitrary, the observational evidence for introducing such parameters is compelling. Perhaps the simplest extension is to break the axisymmetry of the dipole, leaving curtains of accretion in azimuth – models such as these have been proposed by a number of observers attempting to explain variability in CTTSs and are observed in MHD simulations (*Romanova et al.*, 2003). Synthetic time-series for a CTTS magnetosphere structured along these lines were presented by *Symington et al.* (2005a). It was found that some gross characteristics of the observed line profiles were produced using a 'curtains' model, although the general level of variability predicted is larger than that observed, suggesting that the magnetosphere may be characterized by a high degree of axisymmetry, broken by higher-density streams that produce the variability.

The emission line profiles of CTTSs often display the signatures of outflow as well as infall, and recent attempts have been made to account for this in RT modelling. *Alencar et al.* (2005) investigated a dipolar accretion geometry combined with a disk wind in order to model the line profile variability of RW Aur. They discovered that magne-
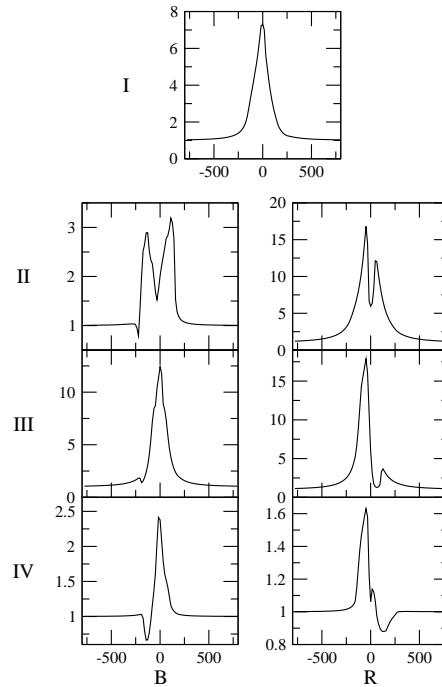
tospheric accretion alone could not simultaneously model Hα, Hβ and NaD profiles, and found that the wind contribution to the lines profiles is quite important in that case.

Hybrid models (*Kurosawa et al.*, 2006) combining a standard dipolar accretion flow with an outflow (e.g., Fig. 6) are capable of reproducing the broad range of observed Hα profiles (Fig. 5). Obviously spectroscopy alone is insufficient to uniquely identify a set of model parameters for an individual object, although by combining spectroscopy with other probes of the circumstellar material, one should be able to reduce the allowable parameter space considerably. For example linear spectropolarimetry provides a unique insight into the accretion process; scattering of the line emission by circumstellar dust imprints a polarization signature on the line which is geometry dependent. An Hα spectropolarimetric survey by *Vink et al.* (2005a) revealed that 9 out of 11 CTTSs showed a measurable change in polarization through the line, while simple numerical models by *Vink et al.* (2005b) demonstrate that this polarization may be used to gauge the size of the disk inner hole.

The radiative-transfer models described above are now routinely used to determine mass accretion rates across the mass spectrum from Herbig AeBe (*Muzerolle et al.*, 2004) stars to brown dwarfs (*Lawson et al.*, 2004; *Muzerolle et al.*, 2005), and in the CTTS mass regime at least the ac-
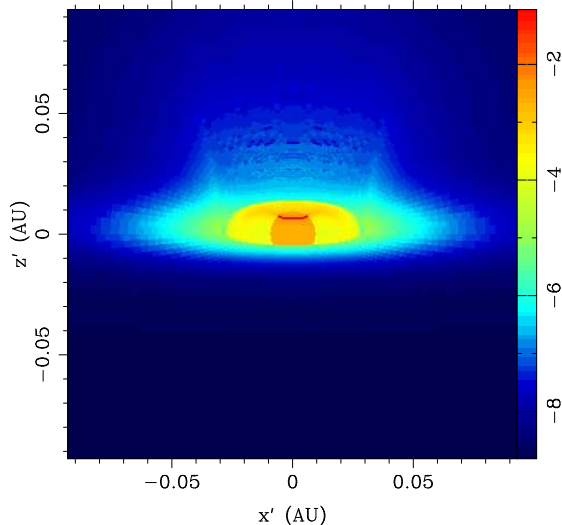
Fig. 6.— A simulated Hα image of an accreting CTTS with an outflow ($\log \dot{M}_{\mathrm{acc}} = -8$, $\log \dot{M}_{\mathrm{wind}} = -9$) viewed at an inclination of $80°$. The wind emission is negligible compared to the emission from the magnetosphere, and the lower half of the wind is obscured by the circumstellar disk (*Kurosawa et al.*, 2006).

cretion rates derived from RT modelling have been roughly calibrated against other accretion-rate measures, such as the UV continuum (e.g., *Muzerolle et al.*, 2001). However, one must be aware of the simplifying assumptions which underlie the models and that must necessarily impact on the validity of any quantity derived from them, particularly the mass accretion rate. Magnetic field measurements (Sect. 2) and time-series spectroscopy (Sect. 4) clearly show us that the geometry of the magnetosphere is far from a pristine axisymmetric dipole, but instead probably consists of many azimuthally distributed funnels of accretion, curved by rotation and varying in position relative to the stellar surface on the timescale of a few stellar rotation periods. Furthermore, the temperature of the magnetosphere and the mass accretion rate are degenerate quantities in the models, with a higher temperature magnetosphere producing more line flux for the same accretion rate. This means that brown dwarf models require a much higher accretion stream temperature than those of CTTSs in order to produce the observed line flux, and although the temperature is grossly constrained by the line broadening (which may preclude lower temperature streams) the thermal structure of the accretion streams is still a problem. Despite these uncertainties, and in defense of the BD models, it should be noted that the low accretion rates derived are consistent with both the lack of optical veiling (*Muzerolle et al.*, 2003a) and the strength of the Ca II λ8662 line (*Mohanty et al.*, 2005).

Current models do not match the line core particularly well, which is often attributed to a break down of the Sobolev approximation; co-moving frame calculations (which are many orders of magnitude more expensive computationally) may be required. An additional problem with current RT modelling is the reliance on fitting a single profile – current studies have almost always been limited to Hα – one that rarely shows an IPC profile (*Edwards et al.*, 1994; *Reipurth et al.*, 1996), is vulnerable to contamination by outflows (e.g., *Alencar et al.*, 2005) and may be significantly spatially extended (*Takami et al.*, 2003). Even in modelling a single line, it is fair to say that the state-of-the-art is some way short of line profile fitting; the best fits reported in the literature may match the observation in terms of peak intensity, equivalent width, or in the line wings, but are rarely convincing reproductions of the observations in detail. Only by simultaneously fitting several lines may one have confidence in the models, particularly if those lines share a common upper/lower level (Hα and Paβ for example). Although such observations are in the literature (e.g., *Edwards et al.*, 1994; *Folha and Emerson*, 2001) their usefulness is marginalized by the likely presence of significant variability between the epochs of the observations at the different wavelengths: simultaneous observations of a wide range of spectral diagnostics are required. Despite the caveats described above, line profile modelling remains a useful (and in the BD case the only) route to the mass accretion rate, and there is real hope that the current factor ~ 5 uncertainties in mass accretion rates derived from RT modelling may be significantly reduced in the future.

4. OBSERVATIONAL EVIDENCE FOR MAGNETOSPHERIC ACCRETION

Observations seem to globally support the magnetospheric accretion concept in CTTSs, which includes the presence of strong stellar magnetic fields, the existence of an inner magnetospheric cavity of a few stellar radii, magnetic accretion columns filled with free falling plasma, and accretion shocks at the surface of the stars. While this section summarizes the observational signatures of magnetospheric accretion in T Tauri stars, there is some evidence that the general picture applies to a much wider range of mass, from young brown dwarfs (*Muzerolle et al.*, 2005; *Mohanty et al.*, 2005) to Herbig Ae-Be stars (*Muzerolle et al.*, 2004; *Calvet et al.*, 2004; *Sorelli et al.*, 1996).

In recent years, the rapidly growing number of detections of strong stellar magnetic fields at the surface of young stars seem to put the magnetospheric accretion scenario on a robust ground (see Sect. 2). As expected from the models, given the typical mass accretion rates (10^{-9} to 10^{-7} M$_\odot$ yr^{-1}, *Gullbring et al.*, 1998) and magnetic field strengths (2 to 3 kG, *Valenti and Johns-Krull*, 2004) obtained from the observations, circumstellar disk inner holes of about 3-9 R$_*$ are required to explain the observed line widths of the CO fundamental emission, that likely come from gas in Keplerian rotation in the circumstellar disk of CTTSs (*Najita et al.*, 2003). There has also been evidence for accretion columns through the common occurrence of inverse P Cygni profiles with redshifted absorptions reaching several

hundred km s^{-1}, which indicates that gas is accreted onto the star from a distance of a few stellar radii (*Edwards et al.*, 1994).

Accretion shocks are inferred from the rotational modulation of light curves by bright surface spots (*Bouvier et al.*, 1995) and modelling of the light curves suggests hot spots covering about one percent of the stellar surface. The theoretical prediction of accretion shocks and its associated hot excess emission are also supported by accretion shock models that successfully reproduce the observed spectral energy distributions of optical and UV excesses (*Calvet and Gullbring*, 1998; *Ardila and Basri*, 2000; *Gullbring et al.*, 2000). In these models, the spectral energy distribution of the excess emission is explained as a combination of optically thick emission from the heated photosphere below the shock and optically thin emission from the preshock and postshock regions. *Gullbring et al.* (2000) also showed that the high mass accretion rate CTTSs have accretion columns with similar values of energy flux as the moderate to low mass accretion rate CTTSs, but their accretion columns cover a larger fraction of the stellar surface (filling factors ranging from less than 1% for low accretors to more than 10% for the high one). A similar trend was observed by *Ardila and Basri* (2000) who found, from the study of the variability of IUE spectra of BP Tau, that the higher the mass accretion rate, the bigger the hot spot size.

Statistical correlations between line fluxes and mass accretion rates predicted by magnetospheric accretion models have also been reported for emission lines in a broad spectral range, from the UV to the near-IR (*Johns-Krull et al.*, 2000; *Beristain et al.*, 2001; *Alencar and Basri*, 2000; *Muzerolle et al.*, 2001; *Folha and Emerson*, 2001). However, in recent years, a number of observational results indicate that the idealized steady-state axisymmetric dipolar magnetospheric accretion models cannot account for many observed characteristics of CTTSs.

Recent studies showed that accreting systems present strikingly large veiling variability in the near-IR (*Eiroa et al.*, 2002; *Barsony et al.*, 2005), pointing to observational evidence for time variable accretion in the inner disk. Moreover, the near-IR veiling measured in CTTSs is often larger than predicted by standard disk models (*Folha and Emerson*, 1999; *Johns-Krull and Valenti*, 2001). This suggests that the inner disk structure is significantly modified by its interaction with an inclined stellar magnetosphere and thus departs from a flat disk geometry. Alternatively, a "puffed" inner disk rim could result from the irradiation of the inner disk by the central star and accretion shock (*Natta et al.* 2001; *Muzerolle et al.*, 2003b). In mildly accreting T Tauri stars, the dust sublimation radius computed from irradiation models is predicted to lie close to the corotation radius (3-9 R$_*$ $\simeq$ 0.03-0.08 AU) though direct interferometric measurements tend to indicate larger values (0.08-0.2 AU, *Akeson et al.*, 2005).

Observational evidence for an inner disk warp has been reported by *Bouvier et al.* (1999, 2003) for AA Tau, as expected from the interaction between the disk and an *in-*
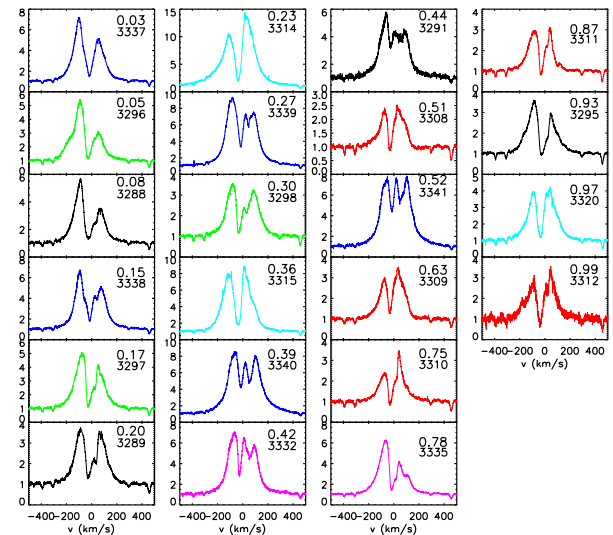

Fig. 7.— The rotational modulation of the Hα line profile of the CTTS AA Tau (8.2d period). Line profiles are ordered by increasing rotational phase (top panel number) at different Julian dates (bottom panel number). Note the development of a high velocity redshifted absorption component in the profile from phase 0.39 to 0.52, when the funnel flow is seen against the hot accretion shock (from *Bouvier et al.*, in prep.).

clined stellar magnetosphere (see Sect. 5). Inclined magnetospheres are also necessary to explain the observed periodic variations over a rotational timescale in the emission line and veiling fluxes of a few CTTSs (*Johns and Basri*, 1995; *Petrov et al.*, 1996; 2001; *Bouvier et al.*, 1999; *Batalha et al.*, 2002). These are expected to arise from the variations of the projected funnel and shock geometry as the star rotates. An example can be seen in Fig. 7 that shows the periodic modulation of the Hα line profile of the CTTS AA Tau as the system rotates, with the development of a high velocity redshifted absorption component when the funnel flow is seen against the hot accretion shock. Sometimes, however, multiple periods are observed in the line flux variability and their relationship to stellar rotation is not always clear (e.g., *Alencar and Batalha*, 2002; *Oliveira et al.*, 2000). The expected correlation between the line flux from the accretion columns, and the continuum excess flux from the accretion shock is not always present either (*Ardila and Basri*, 2000; *Batalha et al.*, 2002), and the correlations predicted by static *dipolar* magnetospheric accretion models are generally not seen (*Johns-Krull and Gafford*, 2002).

Winds are generally expected to be seen as forbidden emission lines or the blueshifted absorption components of permitted emission lines. Some permitted emission line profiles of high-mass accretion rate CTTSs, however, do not always look like the ones calculated with magnetospheric accretion models and this could be in part due to a strong wind contribution to the emission profiles, given the high optical depth of the wind in these cases (*Muzerolle et al.*,

2001; *Alencar et al.*, 2005). Accretion powered hot winds originating at or close to the stellar surface have recently been proposed to exist in CTTSs with high mass accretion rates (*Edwards et al.*, 2003). These winds are inferred from the observations of P Cygni profiles of the He I line (10780 Å) that present blueshifted absorptions which extend up to -400 km/s. *Matt and Pudritz* (2005) have argued that such stellar winds can extract a significant amount of the star's angular momentum, thus helping regulate the spin of CTTSs. Turbulence could also be important and help explain the very wide ($\pm$ 500 km s^{-1}) emission line profiles commonly observed in Balmer and MgII UV lines (*Ardila et al.*, 2002).

Synoptic studies of different CTTSs highlighted the dynamical aspect of the accretion/ejection processes, which only recently has begun to be studied theoretically by numerical simulations (see Sect. 5). The accretion process appears to be time dependent on several timescales, from hours for non-steady accretion (*Gullbring et al.*, 1996; *Alencar and Batalha*, 2002; *Stempels and Piskunov*, 2002; *Bouvier et al.*, 2003) to weeks for rotational modulation (*Smith et al.*, 1999; *Johns and Basri*, 1995; *Petrov et al.*, 2001), and from months for global instabilities of the magnetospheric structure (*Bouvier et al.*, 2003) to years for EXor and FUor eruptions (e.g., *Reipurth and Aspin*, 2004; *Herbig*, 1989).

One reason for such a variability could come from the interaction between the stellar magnetosphere and the inner accretion disk. In general, magnetospheric accretion models assume that the circumstellar disk is truncated close to the corotation radius and that field lines threading the disk corotate with the star. However, many field lines should interact with the disk in regions where the star and the disk rotate differentially. Possible evidence has been reported for differential rotation between the star and the inner disk (*Oliveira et al.*, 2000) through the presence of an observed time delay of a few hours between the appearance of high velocity redshifted absorption components in line profiles formed in different regions of the accretion columns. This was interpreted as resulting from the crossing of an azimuthally twisted accretion column on the line of sight. Another possible evidence for twisted magnetic field lines by differential rotation leading to reconnection events has been proposed by *Montmerle et al.* (2000) for the embedded protostellar source YLW 15, based on the observations of quasi-periodic X-ray flaring. A third possible evidence was reported by *Bouvier et al.* (2003) for the CTTS AA Tau. On timescales of the order of a month, they observed significant variations in the line and continuum excess flux, indicative of a smoothly varying mass accretion rate onto the star. At the same time, they found a tight correlation between the radial velocity of the blueshifted (outflow) and redshifted (inflow) absorption components in the Hα emission line profile. This correlation provides support for a physical connection between time dependent inflow and outflow in CTTSs. *Bouvier et al.* (2003) interpreted the flux and radial velocity variations in the framework of magnetospheric

inflation cycles due to differential rotation between the star and the inner disk, as observed in recent numerical simulations (see Sect. 5). The periodicity of such instabilities, as predicted by numerical models, is yet to be tested observationally and will require monitoring campaigns of chosen CTTSs lasting for several months.

5. NUMERICAL SIMULATIONS OF MAGNETO-SPHERIC ACCRETION

Significant progress has been made in recent years in the numerical modeling of magnetospheric accretion onto a rotating star with a dipolar magnetic field. One of the main problems is to find adequate initial conditions which do not destroy the disk in first few rotations of the star and do not influence the simulations thereafter. In particular, one must deal with the initial discontinuity of the magnetic field between the disk and the corona, which usually leads to significant magnetic braking of the disk matter and artificially fast accretion onto the star on a dynamical time-scale. Specific quasi-equilibrium initial conditions were developed, which helped to overcome this difficulty (*Romanova et al.*, 2002). In axisymmetric (2D) simulations, the matter of the disk accretes inward slowly, on a viscous time-scale as expected in actual stellar disks. The rate of accretion is regulated by a viscous torque incorporated into the numerical code through the α prescription, with typically $\alpha_{\rm v} = 0.01-0.03$.

Simulations have shown that the accretion disk is disrupted by the stellar magnetosphere at the magnetospheric or truncation radius R_T, where the gas pressure in the disk is comparable to the magnetic pressure, $P_{ram} = B^2/8\pi$ (see Sect. 2). In this region matter is lifted above the disk plane due to the pressure force and falls onto the stellar surface supersonically along the field lines, forming funnel flows (*Romanova et al.*, 2002). The location of the inner disk radius oscillates as a result of accumulation and reconnection of the magnetic flux at this boundary, which blocks or "permits" accretion (see discussion of this issue below), thus leading to non-steady accretion through the funnel flows. Nevertheless, simulations have shown that the funnel flow is a quasi-stationary feature during at least $50 - 80$ rotation periods of the disk at the truncation radius, P_0, and recent simulations with improved numerical schemes indicate that this structure survives for more than $1,000$ P_0 (*Long et al.*, 2005). Axisymmetric simulations thus confirmed the theoretical ideas regarding the structure of the accretion flow around magnetized CTTSs. As a next step, similar initial conditions were applied to full 3D simulations of disk accretion onto a star with an *inclined* dipole, a challenging problem which required the development of new numerical methods (e.g., the "inflated cube" grid, cf. *Koldoba et al.*, 2002; *Romanova et al.*, 2003, 2004a). Simulations have shown that the disk is disrupted at the truncation radius R_T, as in the axisymmetric case, but the magnetospheric flow to the star is more complex. Matter flows
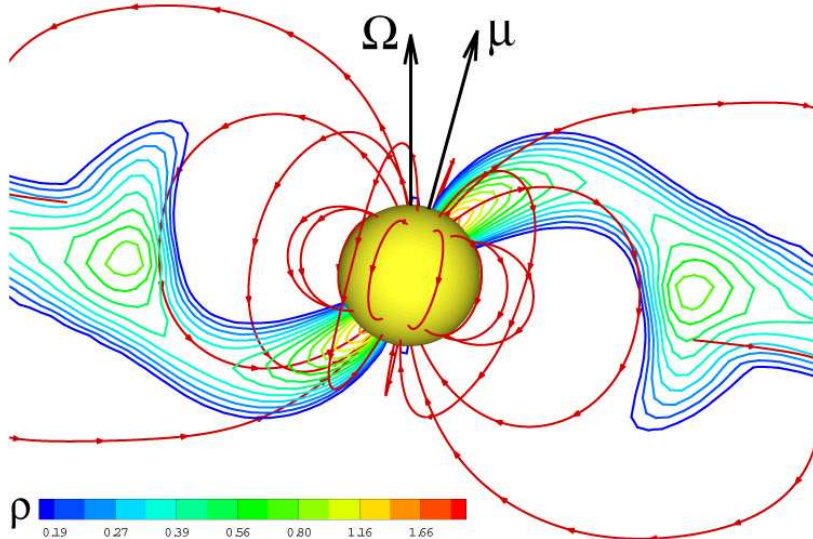
Fig. 8.— A slice of the funnel stream obtained in 3D simulations for an inclined dipole ($\Theta = 15°$). The contour lines show density levels, from the minimum (dark) to the maximum (light). The corona above the disk has a low-density but is not shown. The thick lines depict magnetic field lines (from *Romanova et al.*, 2004a).

around the magnetosphere and falls onto the stellar surface supersonically. The magnetospheric structure varies depending on the misalignment angle of the dipole, but settles into a quasi-stationary state after a few P_0, as demonstrated by recent simulations run up to $40\ P_0$ (*Kulkarni and Romanova*, 2005). In both, 2D and 3D simulations the fluxes of matter and angular momentum to or from the star vary in time, however they are smooth on average. This average value is determined by the properties of the accretion disk.

Numerical simulation studies have shown that a star may either spin up, spin down or be in rotational equilibrium when the net torque on the star vanishes. Detailed investigation of the rotational equilibrium state has shown that the rotation of the star is then *locked* at an angular velocity Ω_{eq} which is smaller by a factor of $\sim 0.67 - 0.83$ than the angular velocity at the truncation radius (*Long et al.*, 2005). The corresponding "equilibrium" corotation radius $R_{CO} \approx (1.3 - 1.5)\ R_T$ is close to that predicted theoretically (e.g., *Ghosh and Lamb*, 1978,1979b; *Königl*, 1991). Recently, the disk-locking paradigm was challenged by a number of authors (e.g., *Agapitou and Papaloizou*, 2000; *Matt and Pudritz*, 2004, 2005). The skepticism was based on the fact that the magnetic field lines connecting the star to the disk may inflate and open, (e.g., *Aly and Kuijpers*, 1990; *Lovelace et al.*, 1995; *Bardou*, 1999; *Uzdensky et al.*, 2002), resulting in a significant decrease of angular momentum transport between the star and the disk. Such an opening of field lines was observed in a number of simulations (e.g., *Miller and Stone*, 1997; *Romanova et al.*, 1998; *Fendt and Elstner*, 2000). Several factors, however, tend to restore an efficient disk-star connection. One of them is that the inflated field lines have a tendency to reconnect and close again (*Uzdensky et al.*, 2002). Furthermore, there is always

a region of closed field lines connecting the inner regions of the disk with the magnetosphere, which provides angular momentum transport between the disk and the star (e.g., *Pringle and Rees*, 1972; *Ghosh and Lamb*, 1979b). This is the region where matter accretes through funnel flows and efficiently transports angular momentum to or from the star. This torque tends to bring a star in co-rotation with the inner regions of the disk. There is always, however, a smaller but noticeable negative torque either connected with the region $r > R_{CO}$ (*Ghosh and Lamb*, 1978,1979b), if the field lines are closed in this region, or associated to a wind which carries angular momentum out along the open field lines connecting the star to a low-density corona. Simulations have shown that the wind is magnetically-dominated (*Long et al.*, 2005; *Romanova et al.*, 2005), though the possibility of an accretion-driven *stellar* wind has also been discussed (*Matt and Pudritz*, 2005). The spin-down through magnetic winds was proposed earlier by *Tout and Pringle* (1992). Both torques are negative so that in rotational equilibrium a star rotates *slower* than the inner disk. Thus, the result is similar to the one predicted earlier theoretically, though the physics of the spin-down contribution may be different. Axisymmetric simulations of the *fast rotating* CTTSs have shown that they efficiently spin-down through both disk-magnetosphere interaction and magnetic winds (*Romanova et al.*, 2005; *Ustyugova et al.*, 2006). For instance, it was shown that a CTTS with an initial period $P = 1$ d spins down to the typically observed periods of about a week in less that 10^6 yr.

Three-dimensional (3D) simulations of disk accretion onto a star with a misaligned dipolar magnetic field have shown that at the non-zero misalignment angle Θ, where Θ is an angle between the magnetic moment μ_* and the rota-
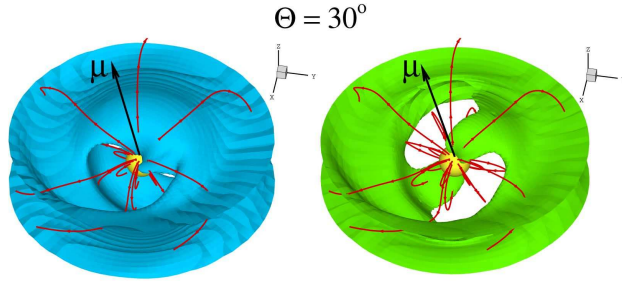
$\Theta = 30^o$

Fig. 9.— 3D simulations show that matter accretes onto the star through narrow, high density streams (right panel) surrounded by lower density funnel flows that blanket nearly the whole magnetosphere (left panel).
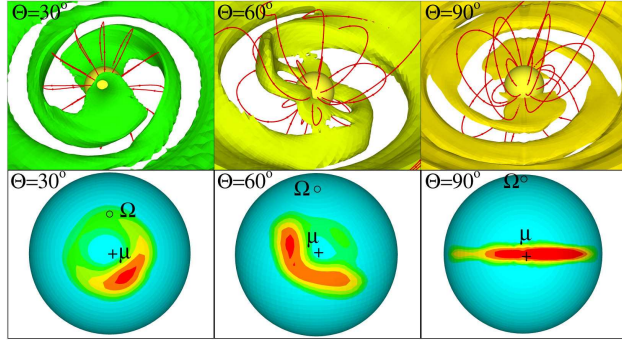

Fig. 10.— Top panels: matter flow close to the star at different misalignment angles Θ. Bottom panels: the shape of the corresponding hot spots. Darker regions correspond to larger density. (From *Romanova et al.*, 2004a).

tional axis $\mathbf{\Omega}_*$ of the star (with the disk axis aligned with $\mathbf{\Omega}_*$), matter typically accretes in two and, in some cases, in several streams (*Koldoba et al.*, 2002; *Romanova et al.*, 2003, 2004a). Figure 8 shows a slice of the magnetospheric stream at $\Theta = 15°$. The density and pressure of the flow increase towards the star as a result of the convergence of the flow. They are also larger in the central regions of the funnel streams. Thus, the structure of the magnetospheric flow depends on the density. The high density part is channeled in narrow funnel streams, while the low density part is wider, with accreting matter blanketting the magnetosphere nearly completely (*Romanova et al.*, 2003, see Figure 9). The spectral lines which form in the funnel streams are redshifted or blueshifted depending on the angle Θ and viewing angle i and their strength is modulated by the rotation of the star.

Matter in the funnel flows falls onto the star's surface and forms *hot spots*. The shape of the spots and the distribution of different parameters (density, velocity, pressure) in the spots reflect those in the cross-section of the funnel streams (*Romanova et al.*, 2004a). Figure 10 shows an example of magnetospheric flows and hot spots at different Θ. At relatively small angles, $\Theta \lesssim 30°$, the spots have the shape of a bow, while at very large angles, $\Theta \gtrsim 60°$, they have a shape

of a bar crossing the surface of the star near the magnetic pole. The density, velocity and pressure are the largest in the central regions of the spots and decrease outward (see Figure 10). The temperature also increases towards the center of the spots because the kinetic energy flux is the largest there. The rotation of the star with surface hot spots leads to variability with one or two peaks per period depending on Θ and i. The two peaks are typical for larger Θ and i. The position of the funnel streams on the star is determined by both the angular velocity of the star and that of the inner radius of the disk. In the rotational equilibrium state, the funnel flows usually settle in a particular "favorite" position. However, if the accretion rate changes slightly, say, increases, then the truncation radius decreases accordingly and the angular velocity at the foot-point of the funnel stream on the disk is larger. As a result, the other end of the stream at the surface of the star changes its position by a small amount. Thus, the location of the spots "wobbles" around an equilibrium position depending on the accretion rate (*Romanova et al.*, 2004a). The variation of the accretion rate also changes the size and the brightness of the spots.

The disk-magnetosphere interaction leads to the thickening of the inner regions of the disk which eases the lifting of matter to the funnel flow. Matter typically accumulates near the closed magnetosphere forming a denser ring (*Romanova et al.*, 2002) which brakes into a spiral structure in case of misaligned dipole (*Romanova et al.*, 2003, 2004a). Typically, two trailing spiral arms are obtained (see Figure 10). 3D simulations have also shown that when accretion occurs onto a tilted dipole, the inner regions of the disk are slightly warped. This results from the tendency of disk material to flow along the magnetic equator of the misaligned dipole (*Romanova et al.*, 2003). Such a warping is observed for medium misalignment angles, $30° < \Theta < 60°$. Disk warping in the opposite direction (towards magnetic axis of the dipole) was predicted theoretically when the disk is strongly diamagnetic (*Aly*, 1980; *Lipunov and Shakura*, 1980; *Lai*, 1999). The warping of the inner disk and the formation of a spiral structure in the accretion flow may possibly be at the origin of the observed variability of some CTTSs (*Terquem and Papaloizou*, 2000; *Bouvier et al.*, 2003).

Progress has also been made in the modeling of outflows from the vicinity of the magnetized stars. Such outflows may occur from the disk-magnetosphere boundary (*Shu et al.*, 1994), from the disk (*Blandford and Payne*, 1982; *Pudritz and Norman*, 1986; *Lovelace et al.*, 1991; *Lovelace et al.*, 1995; *Casse and Ferreira*, 2000; *Pudritz et al.*, 2006), or from the star (*Matt and Pudritz*, 2005). Magneto-centrifugally driven outflows were first investigated in pioneering short-term simulations by *Hayashi et al.* (1996) and *Miller and Stone* (1997) and later in longer-term simulations with a fixed disk (*Ouyed and Pudritz*, 1997; *Romanova et al.*, 1997; *Ustyugova et al.*, 1999; *Krasnopolsky et al.*, 1999; *Fendt and Elstner*, 2000). Simulations including feedback on the inner disk have shown that the process of the disk-magnetosphere interaction is non-stationary: the inner radius of the disk oscillates, and matter accretes to the

star and outflows quasi-periodically (*Goodson et al.*, 1997, 1999; *Hirose et al.*, 1997; *Matt et al.*, 2002; *Kato et al.*, 2004; *Romanova et al.*, 2004b; *Von Rekowski and Brandenburg*, 2004; *Romanova et al.*, 2005), as predicted by *Aly and Kuijpers* (1990). The characteristic timescale of variability is determined by a number of factors, including the time-scale of diffusive penetration of the inner disk matter through the external regions of the magnetosphere (*Goodson and Winglee*, 1999). It was earlier suggested that reconnection of the magnetic flux at the disk-magnetosphere boundary may lead to X-ray flares in CTTSs (*Hayashi et al.*, 1996; *Feigelson and Montmerle*, 1999) and evidence for very large flaring structures has been recently reported by *Favata et al.* (2005).

So far simulations were done for a dipolar magnetic field. Observations suggest a non-dipolar magnetic field near the stellar surface (see Sect. 2, and also, e.g., *Safier*, 1998; *Kravtsova and Lamzin*, 2003; *Lamzin*, 2003; *Smirnov et al.*, 2005). If the dipole component dominates on the large scale, many properties of magnetospheric accretion will be similar to those described above, including the structure of the funnel streams and their physical properties. However, the multipolar component will probably control the flow near the stellar surface, possibly affecting the shape and the number of hot spots. Simulations of accretion to a star with a multipolar magnetic field are more complicated, and should be done in the future.

6. CONCLUSIONS

Recent magnetic field measurements in T Tauri stars support the view that the accretion flow from the inner disk onto the star is magnetically controlled. While typical values of 2.5 kG are obtained for photospheric fields, it also appears that the field topology is likely complex on the small-scales ($R \leq R_\star$), while on the larger scale ($R \gg R_\star$) a globally more organized but weaker (~ 0.1 kG) magnetic component dominates. This structure is thought to interact with the inner disk to yield magnetically-channeled accretion onto the star. Observational evidence for magnetospheric accretion in classical T Tauri star is robust (inner disk truncation, hot spots, line profiles) and the rotational modulation of accretion/ejection diagnostics observed in some systems suggests that the stellar magnetosphere is moderately inclined relative to the star's rotational axis. Realistic 3D numerical models have capitalized on the observational evidence to demonstrate that many properties of accreting T Tauri stars could be interpreted in the framework of magnetically-controlled accretion. One of the most conspicuous properties of young stars is their extreme variability on timescales ranging from hours to months, which can sometimes be traced to instabilities or quasi-periodic phenomena associated to the magnetic star-disk interaction.

Much work remains to be done, however, before reaching a complete understanding of this highly dynamical and time variable process. Numerical simulations still have to incorporate field geometries more complex than a tilted dipole, e.g., the superposition of a large-scale dipolar or quadrupolar field with multipolar fields at smaller scales. The modeling of emission line profiles now starts to combine radiative transfer computations in both accretion funnel flows and associated mass loss flows (disk winds, stellar winds), which indeed appears necessary to account for the large variety of line profiles exhibited by CTTSs. These models also have to address the strong line profile variability which occurs on a timescale ranging from hours to weeks in accreting T Tauri stars. These foreseen developments must be driven by intense monitoring of typical CTTSs on all timescales from hours to years, which combines photometry, spectroscopy and polarimetry in various wavelength domains. This will provide strong constraints on the origin of the variability of the various components of the star-disk interaction process (e.g., inner disk in the near-IR, funnel flows in emission lines, hot spots in the optical or UV, magnetic reconnections in X-rays, etc.).

The implications of the dynamical nature of magnetospheric accretion in CTTSs are plentiful and remain to be fully explored. They range from the evolution of stellar angular momentum during the pre-main sequence phase (e.g., *Agapitou and Papaloizou*, 2000), the origin of inflow/ouflow short term variability (e.g., *Woitas et al.*, 2002; *Lopez-Martin et al.*, 2003), the modeling of the near infrared veiling of CTTSs and of its variations, both of which will be affected by a non planar and time variable inner disk structure (e.g., *Carpenter et al.*, 2001; *Eiroa et al.*, 2002), and possibly the halting of planet migration close to the star (*Lin et al.*, 1996).

REFERENCES

Agapitou V. and Papaloizou J. C. B. (2000) *Mon. Not. R. Astron. Soc., 317*, 273-288.
Akeson R. L., Boden A. F., Monnier J. D., Millan-Gabet R., Beichman C., et al. (2005) *Astrophys. J., 635*, 1173-1181.
Alencar S. H. P. and Basri G. (2000) *Astron. J., 119*, 1881-1900.
Alencar S. H. P. and Batalha C. (2002) *Astrophys. J., 571*, 378-393.
Alencar S. H. P., Basri G., Hartmann L., and Calvet N. (2005) *Astron. Astrophys., 440*, 595-608.
Aly J. J. (1980) *Astron. Astrophys., 86*, 192-197.
Aly J. J. and Kuijpers J. (1990) *Astron. Astrophys., 227*, 473-482.
André P. (1987) In *Protostars and Molecular Clouds* (T. Montmerle and C. Bertout, eds.), pp.143-187. CEA, Saclay.
Ardila D. R. and Basri G. (2000) *Astrophys. J., 539*, 834-846.
Ardila D. R., Basri G., Walter F. M., Valenti J. A., and Johns-Krull C. M. (2002) *Astrophys. J., 567*, 1013-1027.
Bardou A. (1999) *Mon. Not. R. Astron. Soc., 306*, 669-674.

Barsony M., Ressler M. E., and Marsh K. A. (2005) *Astrophys. J., 630*, 381-399.

Basri G. and Bertout C. (1989) *Astrophys. J., 341*, 340-358.

Basri G., Marcy G. W., and Valenti J. A. (1992) *Astrophys. J., 390*, 622-633.

Batalha C., Batalha N. M., Alencar S. H. P., Lopes D. F., and Duarte E. S. (2002) *Astrophys. J., 580*, 343-357.

Beristain G., Edwards S., and Kwan J. (2001) *Astrophys. J., 551*, 1037-1064.

Blandford R. D. and Payne D. G. (1982) *Mon. Not. R. Astron. Soc., 199*, 883-903.

Borra E. F., Edwards G., and Mayor M. (1984) *Astrophys. J., 284*, 211-222.

Bouvier J., Chelli A., Allain S., Carrasco L., Costero R., et al. (1999) *Astron. Astrophys., 349*, 619-635.

Bouvier J., Grankin K. N., Alencar S. H. P., Dougados C., Fernàndez M., et al. (2003) *Astron. Astrophys., 409*, 169-192.

Bouvier J., Cabrit S., Fenandez M., Martin E. L., and Matthews J. M. (1993) *Astron. Astrophys., 272*, 176-206.

Bouvier J., Covino E., Kovo O., Martín E. L., Matthews J. M., et al. (1995) *Astron. Astrophys., 299*, 89-107.

Brown D. N. and Landstreet J. D. (1981) *Astrophys. J., 246*, 899-904.

Calvet N. and Gullbring E. (1998) *Astrophys. J., 509*, 802-818.

Calvet N., Muzerolle J., Briceño C., Fernandez J., Hartmann L., et al. (2004) *Astron. J., 128*, 1294-1318.

Camenzind M. (1990) *Rev. Mex. Astron. Astrofis., 3*, 234-265.

Carpenter J. M., Hillenbrand L. A., and Skrutskie M. F. (2001) *Astron. J., 121*, 3160-3190.

Casse F. and Ferreira J. (2000) *Astron. Astrophys. 361*, 1178-1190

Collier Cameron A. C. and Campbell C. G. (1993) *Astron. Astrophys., 274*, 309-318.

Daou A. G., Johns–Krull C. M., and Valenti J. A. (2006) *Astron. J., 131*, 520-526.

Donati J.-F., Semel M., Carter B. D., Rees D. E., and Collier Cameron A. (1997) *Mon. Not. R. Astron. Soc., 291*, 658-682.

Edwards S., Hartigan P., Ghandour L., and Andrulis C. (1994) *Astron. J., 108*, 1056-1070.

Edwards S., Fischer W., Kwan J., Hillenbrand L., and Dupree A. K. (2003) *Astrophys. J., 599*, L41-L44.

Eiroa, C., Oudmaijer R. D., Davies J. K., de Winter D., Garzn F., et al. (2002) *Astron. Astrophys., 384*, 1038-1049.

Favata F., Flaccomio E., Reale F., Micela G., Sciortino S., et al. (2005) *Astrophys. J. Suppl., 160*, 469-502.

Feigelson E. D. and Montmerle T. (1999) *Ann. Rev. Astron. Astrophys., 37*, 363-408.

Fendt C. and Elstner D. (2000) *Astron. Astrophys., 363*, 208-222.

Folha D. F. M. and Emerson J. P. (1999) *Astron. Astrophys., 352*, 517-531.

Folha D. F. M. and Emerson J. P. (2001) *Astron. Astrophys., 365*, 90-109.

Ghosh P. and Lamb F. K. (1978) *Astrophys. J., 223*, L83-L87.

Ghosh P. and Lamb F. K. (1979a) *Astrophys. J., 232*, 259-276.

Ghosh P. and Lamb F. K. (1979b) *Astrophys. J., 234*, 296-316.

Goodson A. P. and Winglee R. M. (1999) *Astrophys. J., 524*, 159-168.

Goodson A. P., Winglee R. M., and Böhm K.-H. (1997) *Astrophys. J., 489*, 199-209.

Goodson A. P., Böhm K.-H. and Winglee R. M. (1999) *Astrophys. J., 524*, 142-158.

Guenther E. W., Lehmann H., Emerson J. P., and Staude J. (1999) *Astron. Astrophys., 341*, 768-783.

Gullbring E., Barwig H., Chen P. S., Gahm G. F., and Bao M. X. (1996) *Astron. Astrophys., 307*, 791-802.

Gullbring E., Hartmann L., Briceño C., and Calvet N. (1998) *Astrophys. J., 492*, 323-341.

Gullbring E., Calvet N., Muzerolle J., and Hartmann L. (2000) *Astrophys. J., 544*, 927-932.

Hartigan P., Edwards S., and Ghandour L. (1995) *Astrophys. J., 452*, 736-768.

Hartmann L., Hewett R., and Calvet N. (1994) *Astrophys. J., 426*, 669-687.

Hayashi M. R., Shibata K., and Matsumoto R. (1996) *Astrophys. J., 468*, L37-L40.

Herbig G. H. (1989) In *Low Mass Star Formation and Pre-main Sequence Objects* (B. Reipurth, ed.), pp.233-246. ESO, Garching.

Herbst W., Bailer-Jones C. A. L., Mundt R., Meisenheimer K., and Wackermann R. (2002) *Astron. Astrophys., 396*, 513-532.

Hirose S., Uchida Y., Shibata K., and Matsumoto R. (1997) *Pub. Astron. Soc. Jap., 49*, 193-205.

Jardine M., Collier Cameron A., and Donati J.-F. (2002) *Mon. Not. R. Astron. Soc., 333*, 339-346.

Johns C. M. and Basri G. (1995) *Astrophys. J., 449*, 341-364.

Johns–Krull C. M. and Gafford A. D. (2002) *Astrophys. J., 573*, 685-698.

Johns–Krull C. M. and Valenti J. A. (2001) *Astrophys. J., 561*, 1060-1073.

Johns–Krull C. M., Valenti J. A., Hatzes A. P., and Kanaan A. (1999a) *Astrophys. J., 510*, L41-L44.

Johns–Krull C. M., Valenti J. A., and Koresko C. (1999b) *Astrophys. J., 516*, 900-915.

Johns-Krull C. M., Valenti J. A., and Linsky J. L. (2000) *Astrophys. J., 539*, 815-833.

Johns–Krull C. M., Valenti J. A., Saar S. H., and Hatzes A. P. (2001) In *Magnetic Fields Across the Hertzsprung-Russell Diagram* (G. Mathys et al., eds.), pp. 527-532. ASP Conf. Series, San Francisco.

Johns–Krull C. M., Valenti J. A., and Saar S. H. (2004) *Astrophys. J., 617*, 1204-1215.

Johnstone R. M. and Penston M. V. (1986) *Mon. Not. R. Astron. Soc., 219*, 927-941.

Johnstone R. M. and Penston M. V. (1987) *Mon. Not. R. Astron. Soc., 227*, 797-800.

Kato Y., Hayashi M. R. and Matsumoto R. (2004) *Astrophys. J., 600*, 338-342.

Koide S., Shibata K., and Kudoh T. (1999) *Astrophys. J., 522*, 727-752.

Koldoba A. V., Romanova M. M., Ustyugova G. V., and Lovelace R. V. E. (2002) *Astrophys. J., 576*, L53 -L56.

Königl. A. (1991) *Astrophys. J., 370*, L39-L43.

Krasnopolsky R., Li Z.-Y., and Blandford R. (1999) *Astrophys. J., 526*, 631-642.

Kravtsova A. S. and Lamzin S. A. (2003) *Astron. Lett., 29*, 612-620.

Kulkarni A. K. and Romanova M. M. (2005) *Astrophys. J., 633*, 349-357.

Kurosawa R., Harries T. J., and Symington N. H. (2006) *Mon. Not. R. Astron. Soc.*, submitted

Lai D. (1999) *Astrophys. J., 524*, 1030-1047.

Lamzin S. A. (2003) *Astron. Reports, 47*, 498-510.

Lawson W. A., Lyo A.-R., and Muzerolle J. (2004) *Mon. Not. R. Astron. Soc., 351*, L39-L43.

Lin D. N. C., Bodenheimer P., and Richardson D. C. (1996) *Na-*

ture, 380, 606-607.

Lipunov V. M. and Shakura N. I. (1980) *Soviet Astronomy Letters, 6*, 14-17.

Long M., Romanova M. M., and Lovelace R. V. E. (2005) *Astrophys. J., 634*, 1214-1222.

López-Martín L., Cabrit S., and Dougados C. (2003) *Astron. Astrophys., 405*, L1-L4.

Lovelace R. V. E., Berk H. L., and Contopoulos J. (1991) *Astrophys. J., 379*, 696-705.

Lovelace R. V. E., Romanova M. M., and Bisnovatyi-Kogan G. S. (1995) *Mon. Not. R. Astron. Soc., 275*, 244-254.

Martin S. C., (1996) *Astrophys. J., 470*, 537-550.

Matt S. and Pudritz R. E. (2004) *Astrophys. J., 607*, L43-L46.

Matt S. and Pudritz R. E. (2005) *Astrophys. J., 632*, L135-L138.

Matt S., Goodson A. P., Winglee R. M., and Böhm K.-H. (2002) *Astrophys. J., 574*, 232-245.

Ménard F. and Bertout C. (1999) In *The Origin of Stars and Planetary Systems* (C. J. Lada and N. D. Kylafis, eds), pp.341. Kluwer Academic Publishers.

Miller K. A. and Stone J. M. (1997) *Astrophys. J., 489*, 890-902.

Mohanty S. M., Jayawardhana R., and Basri G. (2005) *Astrophys. J., 626*, 498-522.

Montmerle T., Koch-Miramond L., Falgarone E., and Grindlay J. E. (1983) *Astrophys. J., 269*, 182-201.

Montmerle T., Grosso N., Tsuboi Y., and Koyama K. (2000) *Astrophys. J., 532*, 1097-1110.

Muzerolle J., Calvet N., and Hartmann L. (2001) *Astrophys. J., 550*, 944-61.

Muzerolle J., Hillenbrand L., Calvet N., Briceño C., and Hartmann L. (2003a) *Astrophys. J., 592*, 266-281.

Muzerolle J., Calvet N., Hartmann L., and D'Alessio P. (2003b) *Astrophys. J., 597*, L149-L152.

Muzerolle J., D'Alessio P., Calvet N., and Hartmann L. (2004) *Astrophys. J., 617*, 406-417.

Muzerolle J., Luhman K. L., Briceño C., Hartmann L., and Calvet N. (2005) *Astrophys. J., 625*, 906-912.

Najita J., Carr J. S. and Mathieu R. D. (2003) *Astrophys. J., 589*, 931-952.

Natta A., Prusti T., Neri R., Wooden D., Grinin V. P., and Mannings V. (2001) *Astron. Astrophys., 371*, 186-197

Oliveira J. M. Foing, B. H., van Loon J. T., and Unruh Y. C. (2000) *Astron. Astrophys., 362*, 615-627.

Ostriker E. C. and Shu F. H. (1995) *Astrophys. J., 447*, 813-828.

Ouyed R. and Pudritz R. E. (1997) *Astrophys. J., 482*, 712-732.

ud Petit P., Donati J.-F., Wade G. A., Landstreet J. D., Bagnulo S., et al. (2004) *Mon. Not. R. Astron. Soc., 348*, 1175-1190.

Petrov P. P., Gullbring E., Ilyin I., Gahm G. F., Tuominen I., et al. (1996) *Astron. Astrophys., 314*, 821-834.

Petrov P. P., Gahm G. F., Gameiro J. F., Duemmler R., Ilyin I. V., et al. (2001) *Astron. Astrophys., 369*, 993-1008.

Pringle J. E. and Rees M. J. (1972) *Astron. Astrophys., 21*, 1P-9P.

Pudritz R. E. and Norman C. A. (1986) *Astrophys. J., 301*, 571-586.

Pudritz R. E., Rogers C. S., and Ouyed R. (2006) *Mon. Not. R. Astron. Soc., 365*, 1131-1148.

Reipurth B. and Aspin C. (2004) *Astrophys. J., 608*, L65-L68.

Reipurth B., Pedrosa A., and Lago M. T. V. T. (1996) *Astron. Astrophys. Suppl., 120*, 229-256.

Romanova M. M., Ustyugova G. V., Koldoba A. V., Chechetkin V. M., and Lovelace R. V. E. (1997) *Astrophys. J., 482*, 708-711.

Romanova M. M., Ustyugova G. V., Koldoba A. V., Chechetkin V. M., and Lovelace R. V. E. (1998) *Astrophys. J., 500*, 703-713.

Romanova M. M., Ustyugova G. V., Koldoba A. V., and Lovelace R. V. E. (2002) *Astrophys. J., 578*, 420-438.

Romanova M. M., Ustyugova G. V., Koldoba A. V., Wick J. V., and Lovelace R. V. E. (2003) *Astrophys. J., 595*, 1009-1031.

Romanova M. M., Ustyugova G. V., Koldoba A. V., and Lovelace R. V. E. (2004a) *Astrophys. J., 610*, 920-932.

Romanova M. M., Ustyugova G. V., Koldoba A. V., and Lovelace R. V. E. (2004b) *Astrophys. J., 616*, L151 -L154.

Romanova M. M., Ustyugova G. V., Koldoba A. V., and Lovelace R. V. E. (2005) *Astrophys. J., 635*, L165-L168.

Safier P. N. (1998) *Astrophys. J., 494*, 336-341.

Shu F., Najita J., Ostriker E., Wilkin F., Ruden S., and Lizano S. (1994) *Astrophys. J., 429*, 781-796.

Smirnov D. A., Lamzin S. A., Fabrika S. N., and Valyavin G. G. (2003) *Astron. Astrophys., 401*, 1057-1061.

Smirnov D. A., Lamzin S. A., Fabrika S. N., and Chuntonov G. A. (2004) *Astron. Lett., 30*, 456-460.

Smirnov D. A., Romanova M. M., and Lamzin S. A. (2005) *Astron. Lett., 31*, 335-339.

Smith K. W., Lewis G. F., Bonnell I. A., Bunclark P. S., and Emerson J. P. (1999) *Mon. Not. R. Astron. Soc., 304*, 367-388.

Smith K., Pestalozzi M., Güdel M., Conway J., and Benz A. O. (2003) *Astron. Astrophys., 406*, 957-967.

Sorelli C., Grinin V. P., and Natta A. (1996) *Astron. Astrophys., 309*, 155-162.

Stempels H. C. and Piskunov N. (2002) *Astron. Astrophys., 391*, 595-608.

Symington N. H., Harries T. J., and Kurosawa R. (2005a) *Mon. Not. R. Astron. Soc., 356*, 1489-1500.

Symington N. H., Harries T. J., Kurosawa R., and Naylor T. (2005b) *Mon. Not. R. Astron. Soc., 358*, 977-984.

Takami M., Bailey J., and Chrysostomou A. (2003) *Astron. Astrophys., 397*, 675-984.

Terquem C. and Papaloizou J. C. B. (2000) *Astron. Astrophys., 360*, 1031-1042.

Tout C. A. and Pringle J. E. (1992) *Mon. Not. R. Astron. Soc., 256*, 269-276.

Ustyugova G. V., Koldoba A. V., Romanova M. M., and Lovelace R. V. E. (1999) *Astrophys. J., 516*, 221-235.

Ustyugova, G.V., Koldoba, A.V., Romanova, M.M., and Lovelace, R.V.E. (2006). *Astrophys. J.*, in press

Uzdensky D. A., Königl A., and Litwin C. (2002) *Astrophys. J., 565*, 1191-1204.

Valenti J. A. and Johns-Krull C. M. (2004) *Astrophys. Sp. Sci. Ser., 292*, 619-629.

Valenti J. A., Basri G., and Johns C. M. (1993) *Astron. J., 106*, 2024-2050.

Vink J. S., Drew J. E., Harries T. J., Oudmaijer R. D., and Unruh Y. (2005a) *Mon. Not. R. Astron. Soc., 359*, 1049-1064.

Vink J. S., Harries T. J., and Drew J. E. (2005b) *Astron. Astrophys., 430*, 213-222.

Vogt S. S. (1980) *Astrophys. J., 240*, 567-584.

von Rekowski B. and Brandenburg A. (2004) *Astron. Astrophys., 420*, 17-32.

Warner B. (2004) *Publ. Astron. Soc. Pac., 116*, 115-132

Woitas J., Ray T. P., Bacciotti F., Davis C. J., and Eislöffel J. (2002) *Astrophys. J., 580*, 336-342.

Yang H., Johns–Krull C. M., and Valenti J. A. (2005) *Astrophys. J., 635*, 466-475.